JACS
JOURNAL OF THE AMERICAN CHEMICAL SOCIETY
Article
pubs.acs.org/JACS

Structure of a Glycomimetic Ligand in the Carbohydrate Recognition Domain of C-type Lectin DC-SIGN. Structural Requirements for Selectivity and Ligand Design

Michel Thépaut,[†,‡,§,▽] Cinzia Guzzi,[⊥,▽] Ieva Sutkeviciute,[†,‡,§] Sara Sattin,[∥] Renato Ribeiro-Viana,[⊥] Norbert Varga,[∥] Eric Chabrol,[†,‡,§] Javier Rojo,[⊥] Anna Bernardi,[∥] Jesus Angulo,[⊥] Pedro M. Nieto,[⊥] and Franck Fieschi*[,†,‡,#]

[†]Institut de Biologie Structurale, Université Grenoble I, 41 rue Jules Horowitz, Grenoble, F-38027, France

[‡]CNRS, UMR 5075, Grenoble, F-38000, France

[§]CEA, DSV, Grenoble, F-38000, France

[∥]Dipartimento di Chimica via Golgi 19, Universita' di Milano, 20133 Milano, Italy

[⊥]Glycosystems Laboratory, Instituto de Investigaciones Químicas (IIQ), CSIC − Universidad de Sevilla, Américo Vespucio 49, 41092 Sevilla, Spain

[#]Institut Universitaire de France, 103 boulevard Saint-Michel 75005 Paris, France

Supporting Information

ABSTRACT: In genital mucosa, different fates are described for HIV according to the subtype of dendritic cells (DCs) involved in its recognition. This notably depends on the C-type lectin receptor, langerin or DC-SIGN, involved in gp120 interaction. Langerin blocks HIV transmission by its internalization in specific organelles of Langerhans cells. On the contrary, DC-SIGN enhances HIV trans-infection of T lymphocytes. Thus, approaches aiming to inhibit DC-SIGN, without blocking langerin, represent attractive anti-HIV strategies. We previously demonstrated that dendrons bearing multiple copies of glycomimetic compounds were able to block DC-SIGN-dependent HIV infection in cervical explant models. Optimization of such ligand requires detailed characterization of its binding mode. In the present work, we determined the first high-resolution structure of a glycomimetic/DC-SIGN complex by X-ray crystallography. This glycomimetic, pseudo-1,2-mannobioside, shares shape and conformational properties with Manα1−2Man, its natural counterpart. However, it uses the binding epitope previously described for Lewis X, a ligand specific for DC-SIGN among the C-type lectin family. Thus, selectivity gain for DC-SIGN versus langerin is observed with pseudo-1,2-mannobioside as shown by surface plasmon resonance analysis. In parallel, ligand binding was also analyzed by TR-NOESY and STD NMR experiments, combined with the CORCEMA-ST protocol. These studies demonstrate that the complex, defined by X-ray crystallography, represents the unique binding mode of this ligand as opposed to the several binding orientations described for the natural ligand. This exclusive binding mode and its selective interaction properties position this glycomimetic as a good lead compound for rational improvement based on a structurally driven approach.

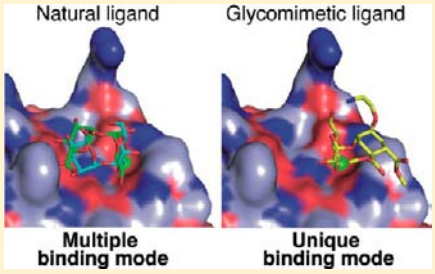

INTRODUCTION

Dendritic cells (DCs) are key players in the initial response to pathogens as they are the first participants in the long series of events in host−pathogen interaction leading to activation of specific T-cells.[1,2] They are found in epidermal and mucosal tissues and are thus able to quickly recognize new invading pathogens through the identification of pathogen associated molecular patterns (PAMPs). The efficacy of DCs in their sentinel role is related to the wide diversity of pattern recognition receptors (PRRs) they express on their surface. Apart from the Toll Like receptors family of PRRs, they also possess C-type lectin receptors (CLRs) dedicated to the specific recognition of pathogen carbohydrate patterns.[3] Among these CLRs, DC-SIGN (dendritic cell-specific ICAM-3 grabbing nonintegrin) has attracted a great deal of attention during the past decade. Initially highlighted for its role in HIV transmission to T cells,[4] it has then been identified as a PRR hijacked by many other pathogens, for instance, some viruses, bacteria, fungi, and parasites, to escape immune response in their infectious processes.[5,6] More recently, DC-SIGN has also been involved in the modulation of the immune response.[7]

DC-SIGN is a type II transmembrane protein with a short cytosolic region, a transmembrane segment, and an extended extracellular domain (ECD) projecting its carbohydrate binding domain up to 320 Å above the cell surface, as a bait to trap potential antigens.[8] This extracellular domain is divided into two structurally and functionally distinct regions: a neck region,

Received: June 1, 2012
Published: January 29, 2013

   dx.doi.org/10.1021/ja3053305 | J. Am. Chem. Soc. 2013, 135, 2518−2529

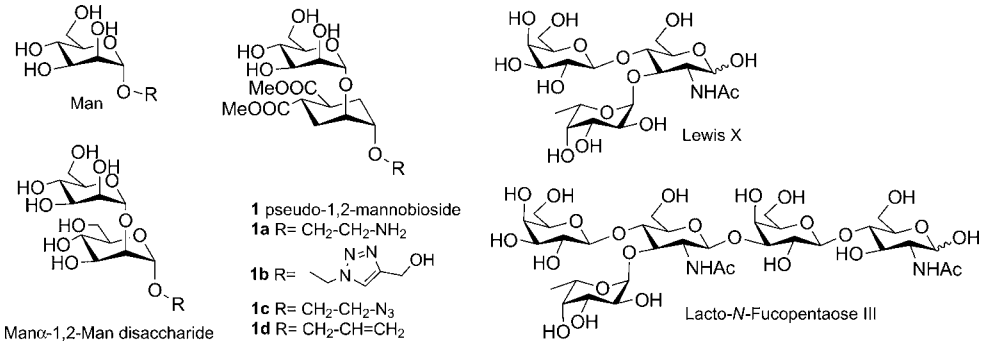

Figure 1. Structure of compounds used or discussed in this study.

involved in the tetramerization of the receptor, and a calcium-dependent carbohydrate recognition domain (CRD), which is at the heart of the molecular recognition processes mediated by DC-SIGN.

Therefore, many groups are developing strategies to block the sugar binding site within DC-SIGN CRD to prevent its use by pathogens' glycoproteins.[9−12] DC-SIGN/pathogen interactions are complex and imply multipoint attachment benefiting from the DC-SIGN tetrameric state and from its organization into clustered patches at the cell membrane.[13,14] For this reason, almost all of these inhibition strategies exploit a multiple ligand presentation platform (polymers, dendrimers, or nanoparticles), on which the relevant ligands are presented for interaction with DC-SIGN CRD.[15−18] Several "proof of concept" studies have been performed using a simple mannose as grafted ligands onto these various display systems.[9,11,19] Indeed, we initially demonstrated that dendrimers loaded with multiple copies of mannose were able to inhibit DC-SIGN/gp120 interaction.[9] However, mannose, as natural ligand, is not specific enough for in vivo practical applications. The design of a ligand with good selectivity and basal affinity is of crucial importance. Several groups have invested efforts in DC-SIGN ligand improvements by increasing the complexity of the oligosaccharide (reconstructing natural high mannose oligosaccharide, for instance[10,15,17]), by selecting nonsugar molecules with high throughput screening[20,21] or by designing new synthetic molecules mimicking natural sugar properties.[22−25]

On the basis of two natural ligands, Manα1−2Man disaccharide and Lewis X trisaccharide, we have developed glycomimetic compounds that have good affinity for DC-SIGN and low structural complexity. In the mannose series (Figure 1), we recently demonstrated that dendrons or dendrimers bearing multiple copies of pseudo-1,2-mannobioside (**1**) were able to block DC-SIGN-dependent HIV trans-infection of T cells,[16] HIV infection in cervical explant models,[26] and Ebola-pseudotyped viral infection.[18]

We also developed a class of Lewis X mimics containing a fucosylamide anchor and demonstrated their potential in terms of specificity toward DC-SIGN relative to langerin, a related lectin.[25] Because of their chemical stability, resistance to enzymatic degradation by glycosidases,[27] and their rather simple and high yield synthetic route, these glycomimetics of first generation represent good candidates for optimization leading to efficient specific inhibitors for DC-SIGN.

To enable ligand improvement, a good knowledge of the particular binding mode of model compounds is of the utmost importance. To achieve this goal, glycoscientists often face a particularly hard and specific task given by the nature of glycan/protein interactions. Indeed, oligosaccharide ligands often have several binding modes within a single binding site in Ca^{2+}-dependent lectins.[28−30] Moreover, computational tools are often of limited use in the prediction of sugar−lectin interaction modes due to the peculiar properties of lectin binding sites. As a consequence, ligand modifications aiming to improve one binding mode may disfavor another, leading to unpredictable global effects on the affinity for the receptor. Therefore, the optimization process becomes a challenge. For DC-SIGN, it has been shown that the natural ligand Manα1−2Man disaccharide displays at least two different binding modes within the Ca^{2+} binding site:[28,29] the major mode is achieved by coordination to the Ca^{2+} atom of the 3-OH and 4-OH equatorial groups of the reducing end mannose residue, while the minor one occurs through the same groups of the nonreducing end mannose ring. The pseudo-1,2-mannobioside **1** and the natural mannobioside Manα1−2Man are known to share a similar shape and similar conformational properties.[27] However, **1** contains a single mannose unit at the nonreducing end and could be expected to bind DC-SIGN similarly to the minor binding mode of Manα1−2Man. Preliminary docking and NMR analysis of its binding properties to DC-SIGN suggested that several orientations of the ligand within the binding site were still possible, and none could be selected on the basis of the available data.[22]

In the present work, we describe the first high-resolution structure of a glycomimetic ligand in complex with DC-SIGN. Using X-ray crystallography on crystallized DC-SIGN CRD/**1** complex, we have been able to characterize at a molecular level an unpredicted binding mode for such compound with the CRD. To obtain a dynamic picture of the interaction in solution, ligand binding was also analyzed by NMR spectroscopy. Transfer NOE (TR-NOESY) and saturation transfer difference (STD) NMR experiments were used combined with the CORCEMA-ST protocol, which enables prediction of STD intensities from the Cartesian atomic coordinates of the ligand−receptor complex. These studies demonstrated that in solution **1** binds as observed in the solid state, and therefore the complex defined by X-ray represents the unique binding mode of this ligand in the Ca^{2+} binding site of DC-SIGN. Because of this exclusive binding mode, this ligand represents a good lead compound for a rational ligand optimization procedure, and the X-ray structure reported here represents a powerful tool for virtual screening and docking as a guide to new chemical improvement of this compound.

In addition, the structural analysis of this first high-resolution glycomimetics/DC-SIGN complex, as well as its comparison with other lectin binding sites, sets the basis for the design of efficient and specific DC-SIGN inhibitors. In particular, the interaction of **1** with langerin was also examined by SPR,

dx.doi.org/10.1021/ja3053305 | J. Am. Chem. Soc. 2013, 135, 2518−2529

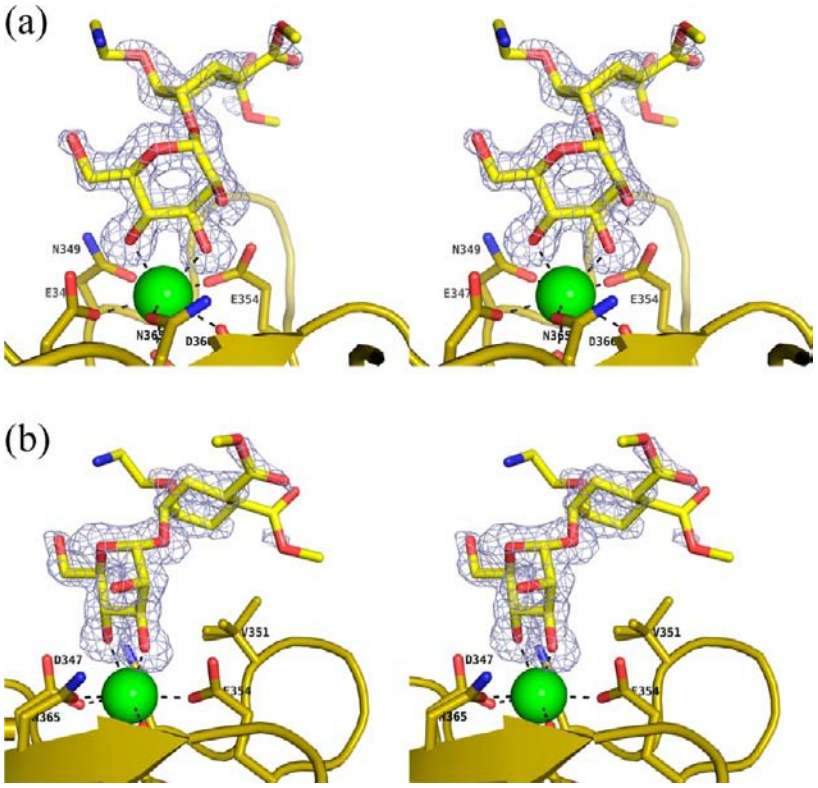

Figure 2. Stereo views of electron density maps for bound pseudo-1,2-mannobioside. (a) and (b) correspond to two different orientations. The bound ligand is shown superimposed on the $F_o - F_c$ electron density map (gray, 3σ contour). Residues involved in Ca^{2+} binding are visualized and labeled. V351 exhibits two alternative conformations with 50% occupancy in the crystal structure. Both of them are represented in (b).

leading to the satisfactory conclusion that **1** present improved selectivity for DC-SIGN. Langerin, a mannose binding C-type lectin expressed on Langerhans cells,[31] is present in the same mucosal environment as interstitial DCs expressing DC-SIGN, but it is known to possess a protective action against HIV infection, which should not be antagonized by therapeutic entities targeted against DC-SIGN.[32] It was recently reported that langerin binds effectively to Manα1−2Man containing oligosaccharides, and the X-ray structure of this protein in complex with the Manα1−2Man disaccharide was described.[33] Thus, the conclusion that **1** is a selective DC-SIGN binder is nontrivial and of great importance for further improvement en route to a potential therapeutic use of these Man-based glycomimetics in the prevention of sexually transmitted HIV infection.

RESULTS AND DISCUSSION

X-ray Crystal Structure of the Complex of DC-SIGN CRD with Pseudo-1,2-mannobioside 1a. To characterize the binding mode of the glycomimetics and to acquire structural data for the optimization process, cocrystallization experiments of DC-SIGN CRD with some of the produced glycomimetic compounds were assayed. Crystals of monomeric DC-SIGN CRD in the presence of pseudo-1,2-mannobioside **1a** (Figure 1) were obtained in crystallization conditions derived from those reported for the DC-SIGN CRD/Manα1−2Man.[28] The crystals contain one copy of the CRD in the asymmetric unit with a $P4_32_12$ space group.

After structure resolution from a model without sugar, an electron density was observed on the Ca^{2+} ion, confirming the presence of the pseudosugar in the canonical carbohydrate binding site of the CRD (Figure 2A). The structure of this complex has been solved at 1.42 Å resolution. Comparison with previously reported structures of DC-SIGN complexes, with natural ligands such as Manα1−2Man (pdb code: 2IT6) or Lewis X derivatives (pdb code: 1SL5), shows that structures of the proteins, and more particularly residues involved in the binding site, are well conserved as illustrated by RMSD of 0.322 and 0.449 Å with respect to 2IT6 and 1SL5, respectively, for the backbone atoms (see also the Supporting Information for detailed comparison, Figure S1). As for many other mannose-based ligands, **1a** directly binds to the Ca^{2+} ion through coordination bonds with equatorial 3-OH and 4-OH groups of the nonreducing mannose unit. The mannose unit, as well as the cyclohexane ring, is clearly visualized, as shown by the electron density map (Figure 2). On the contrary, the electron density of the dimethyl ester substituents on the cyclohexane moiety (Figure 2) as well as the ethylamine appendage are poorly or not visible, suggesting that these parts of the molecule remain flexible within the complex. Three water molecules are associated with the ligand, and only one of them connects the molecule, from its 2-OH, to the protein residue D367 (see Supporting Information, Figure S2).

Mannose 3-OH and 4-OH groups also interact with the Ca^{2+} ligand residues Glu 347, Asn 349, Glu 354, and Asn 365 through hydrogen bonds, and an additional interaction is observed between the 2-OH group of the mannose unit and Asn 365. The cyclohexane ring of the ligand contributes exclusively to the binding through van der Waals contacts with Val 351 side chain. The conformation of the ligand corresponds to the extended conformation (φ O5−C1−O2′−C2′ is 66.3°; ψ' C1−O2′−C2′−C1′ is −141.11°) that has been described as the most abundant in solution for the mimic.[27] The ethylamine linker on the cyclohexane is free to move and oriented toward

dx.doi.org/10.1021/ja3053305 | J. Am. Chem. Soc. 2013, 135, 2518−2529

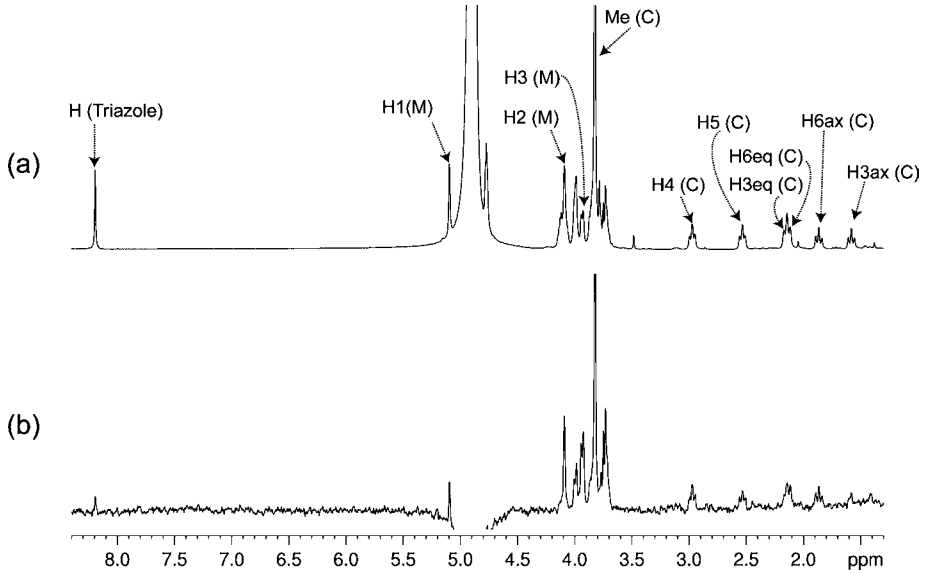

Figure 3. STD NMR study of the interaction of ligand **1b** with DC-SIGN in solution. (a) ^{1}H NMR reference spectrum (off-resonance frequency 40 ppm) and (b) STD spectrum (on-resonance frequency 0 ppm) of a sample containing 1 mM of **1b** and 19 μM of DC-SIGN ECD, at 25 °C (500 MHz). Key proton signals are labeled in (a).

the solvent, far from the protein surface. This suggests that functionalization of the pseudo-1,2-mannobioside through this position onto multivalent presenting scaffolds should not affect the observed binding mode in solution. Indeed, the crystal structure of the DC-SIGN CRD/pseudo-1,2-mannobioside observed here may represent a good starting point for molecular improvement.

NMR Analysis of the Interaction of Pseudo-1,2-mannobioside with DC-SIGN in Solution. Previous examples demonstrated that DC-SIGN recognizes carbohydrate ligands in a multimodal fashion, whereas X-ray diffraction studies can only show one of the possible bound poses, losing the structural information on other conformers and/or the other binding modes.[28] Despite the high resolution of DC-SIGN/ligands complex structures solved by X-ray crystallography, additional approaches have been crucial to get a deeper structural insight to carbohydrate/lectin binding modes. Particularly, in a previous work, STD NMR enabled the characterization of both binding modes of a synthetic Manα1−2Man disaccharide,[29] while the X-ray study was not able to fully determine the second binding mode.[28] This multimodal binding feature seems to be a common characteristic of DC-SIGN for its ligands, as NMR data on the molecular recognition between this lectin and other synthetic glycan mimics have also revealed multiple binding modes of the ligands.[30] Taking into account the above considerations, a quantitative comparison between the X-ray data obtained for the DC-SIGN/**1a** complex with data from STD NMR studies in solution was planned. The binding of **1a** has been previously studied by STD NMR techniques,[22] but the epitope was not fully characterized due to a strong spectral overlap of the NMR signals. The methylene protons in the cyclohexane unit (H3(C) and H6(C), both axial and equatorial) appeared at degenerated chemical shifts, precluding individual integration of their STD signals. In the course of parallel studies in the laboratory, ligand **1c** (R = $CH_2-CH_2-N_3$) was used to prepare multivalent glycodendrimers via 1,3-dipolar cycloaddition catalyzed by Cu(I), a "click chemistry" reaction. This approach produced the formation of a triazole ring, which induced a significant chemical shift variation of some key signals corresponding to the cyclohexane unit, leading to a better spectral dispersion.

Thus, we modified the structure of **1** including a triazole ring in the spacer at the pseudoanomeric position, generating compound **1b**. This modification was expected to help signal analysis, without modifying the interaction mode of the ligand with the protein. Indeed, the NMR data (Figure 3) support this hypothesis: the triazole residue did not affect binding to DC-SIGN neither in terms of affinity (STD NMR competition experiment, see Figure S3 in the Supporting Information) nor in terms of protein−ligand contacts (the STD signals of the triazole residue were basically null, and the pattern of intensities comparable to that of ligand **1a**; compare Figure 4 and previously described STD signals for **1a**[22]). Furthermore, as expected, this monovalent compound showed chemical shifts similar to those observed in the multivalent systems with little signal overlapping in the ^{1}H NMR spectrum and, in particular, well-resolved signals for protons H3ax(C) and H6ax(C). Therefore, compound **1b** turned out to be a very adequate model to study the binding process with DC-SIGN by STD NMR.

The ability to distinguish both axial protons allowed us to demonstrate experimentally that proton H6ax received a considerably larger amount of saturation from the protein than H3ax (Figure 3). In fact, H3ax could not be integrated accurately in the STD spectrum due to its low signal-to-noise ratio, while H6ax showed the strongest STD intensity among the ligand protons, along with the mannose proton H3(M). This result indicated that H6ax(C) is in very close contact with nonexchangeable protons of some side chains of the protein binding pocket in the bound state. Interestingly, inspection of the structure of the complex obtained by X-ray diffraction (Figure 2) leads to a straightforward explanation of the strong saturation transferred from the protein to H6ax(C) of **1b**, as this proton sits on top of the methyl groups of the Val 351 side chain. In the experimental setup, irradiation at 0 ppm leads to a very efficient saturation of these methyl protons of DC-SIGN, in agreement with the strong STD effect observed for the adjacent H6ax ligand proton.

dx.doi.org/10.1021/ja3053305 | J. Am. Chem. Soc. 2013, 135, 2518−2529

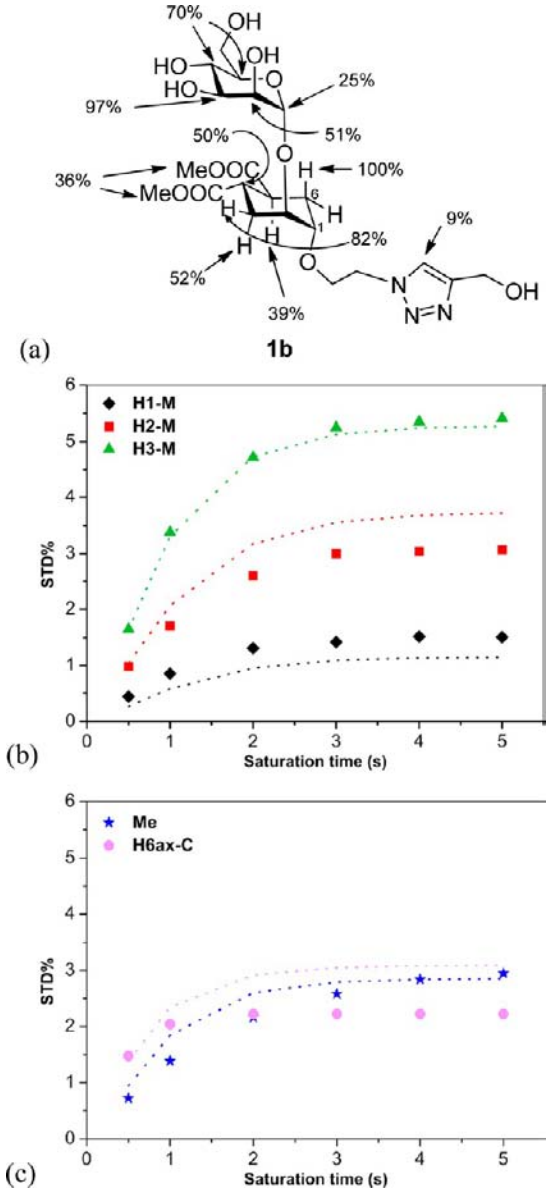

Figure 4. STD growth curves and CORCEMA-ST analysis. (a) Ligand epitope map of **1b** at 25 °C. (b) STD build-up curves of the mannose residue of **1b**, (c) STD build-up curves of the cyclohexyl residue of **1b**. Theoretical STD intensities predicted by CORCEMA-ST using the Cartesian coordinates of the X-ray structure are shown in dashed lines; experimental data are in symbols.

Having defined the binding epitope, a quantitative analysis of the agreement between the determined X-ray structure of the complex and the NMR data in solution was carried out using full matrix relaxation calculations and the Cartesian coordinates from X-ray diffraction (Figure 4). No refinement of the X-ray coordinates was carried out during CORCEMA-ST calculations, and only those protons with the most intense and well-isolated STD signals were considered in the analysis. Figure 4 compares the experimental STD build-up curves with the corresponding theoretical predictions by CORCEMA-ST calculations for the mannose (Figure 4b) and cyclohexyl (Figure 4c) residues of **1b**.[34] A good fit between theoretical and experimental curves is evident, quantitatively confirmed by the resulting low NOE R-factor of 0.2 (see Experimental Procedures).[35,36] This demonstrates that the binding mode of the ligand in solution, as detected by NMR, is the same as the one observed in the crystal. This result strongly supports the notion that DC-SIGN binds this ligand in a single orientation, which corresponds to that observed in the X-ray structure.

We then carried out NOE experiments to investigate the conformation of **1b** in solution, both free and bound to DC-SIGN. A previous study performed on **1d**[27] (differing from **1b** only in the chemical nature of the linker) had identified two conformations E (extended, characterized by the exclusive H1(M)−H3eq(C) NOE contact) and S (stacked, characterized by the exclusive H1(M)−H1(C) NOE contact), as major and minor contributors in solution, respectively. For **1b** the minor S conformer could not be detected in the free state, as the exclusive H1(M)−H1(C) NOE was not observed (see 1D NOESY, Figure S4, in the Supporting Information), indicating that only the extended E conformer is detectable in solution. For the analysis of the free and bound states of the ligand, the resulting 2D NOESY spectra are shown in Figure 5.

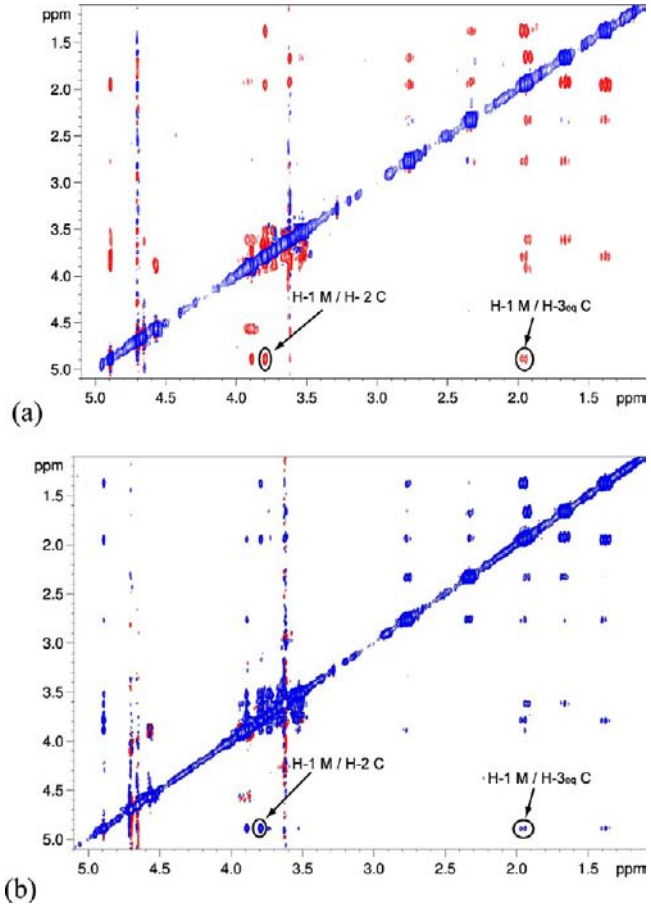

Figure 5. Expansions of NOESY experiments at 25 °C (500 MHz) of **1b**. (a) Free state (1 mM **1b**) mixing time 600 ms. (b) In the presence of 19 μM DC-SIGN ECD, mixing time 300 ms. Labels indicate some key NOE peaks.

We did not carry out a full refinement of the ligand structure in the bound state as the data were affected by some spin diffusion.[37] However, the observation of the strong key interglycosidic cross peaks H1(M)−H2(C), H1(M)−H3eq-(C), and H2(M)−H4(C) in the TR-NOESY spectra is all consistent with the X-ray data and supports the notion that the conformation observed in the X-ray structure is well

dx.doi.org/10.1021/ja3053305 | J. Am. Chem. Soc. 2013, 135, 2518−2529

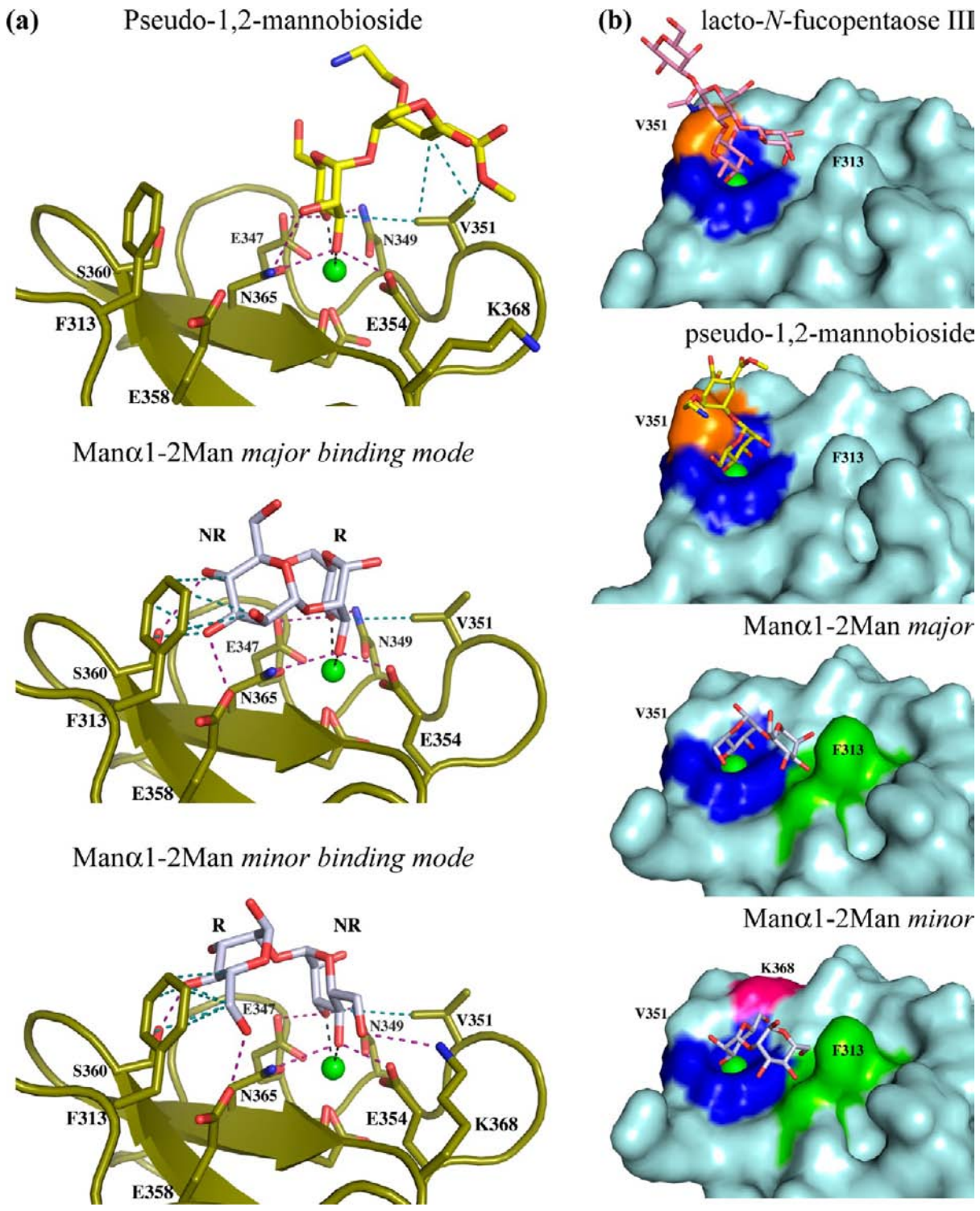

Figure 6. Binding of pseudo-1,2-mannobioside to DC-SIGN and comparison with the binding of other mannose and fucose-based oligosaccharides. (a) Comparison of pseudo-1,2-mannobioside **1a** and Manα1−2Man binding modes. The protein is shown in olive, the pseudo-1,2-mannobioside is in yellow, Manα1−2Man is in light gray, with nitrogen, oxygen, and calcium represented as blue, red, and green spheres, respectively. Hydrogen bonds are shown as dashed purple lines, Ca^{2+} coordination bonds are dashed black lines, and key van der Waals interactions are indicated by dashed blue lines. Both Manα1−2Man binding modes are oriented highlighting the reducing (R) and nonreducing (NR) ends. (b) Comparison of carbohydrate binding surface epitope for LNFP III, pseudo-1,2-mannobioside **1a**, and both binding modes of Manα1−2Man (see Figure 1 for structure of LNFP III). Residues common to binding of all carbohydrates and involved in Ca^{2+} chelation are in dark blue, residues specific for both Manα1−2Man binding modes are in green (F313, S360, and E358), K368 specific for Manα1−2Man minor binding mode is in pink, and V351 involved in LNFPIII and pseudo-1,2-mannobioside **1a** binding is in orange. (a) and (b) are representations with two opposite side views; V351 and P313 are highlighted in (B) for appropriate orientation. In (a) only one of the two alternatives side chain conformations of V351 is represented for clarity.

dx.doi.org/10.1021/ja3053305 | J. Am. Chem. Soc. 2013, 135, 2518−2529

represented for the complex in solution. In fact, the ligand interproton distances experimentally determined from the TR-NOESY experiments, by using the isolated spin pair approximation (ISPA), displayed good agreement with the distances measured on the crystal structure (see Table 2 and the Supporting Information).

Binding Mode Comparison of Pseudo-1,2-mannobioside with Its Natural Model, Manα1−2Man. From the combination of the two biophysical structural approaches described above (X-ray and NMR), we demonstrated a unique binding mode for pseudo-1,2-mannobioside **1** and provided a detailed molecular view of it. Initially, **1** was designed as a structural mimic of Manα1−2Man. Notably, both molecules exhibit an equilibrium between two conformations in solution (stacked and extended) with similar φ and ψ angles around the glycosidic linkage.[27] Two alternative binding modes were previously characterized for Manα1−2Man (Figure 6A)[29] in DC-SIGN, each using a different mannose unit for Ca^{2+} coordination. The absence of hydroxyl groups in the cyclohexane moiety of **1** originally suggested that interaction would occur along the Manα1−2Man minor binding mode (Figure 6A), which involves the nonreducing end mannose and would possibly generate a favorable interaction between F313 of the secondary binding site and the cyclohexane moiety of **1**. Surprisingly, **1** was found to interact through a third, distinct mode: the position of the Ca-binding diol (mannose 3-OH and 4-OH) is swapped relative to the Manα1−2Man complex, so that the 3-OH group of **1** contacts E354 (as opposed to the 4-OH group of Manα1−2Man) and that the 4-OH group of **1** contacts E347 (as opposed to the 3-OH group of Manα1−2Man). The observed conformation of **1** is close to the extended one, and the cyclohexane ring participates in the interaction through van der Waals contacts with V351. Thus, despite their largely documented structural similarity, **1** and Manα1−2Man have totally different DC-SIGN binding modes (Figure 6A and B). On the contrary, strong similarity is observed with the binding epitope of Lewis X derivatives (lacto-*N*-fucopentaose III, 1SL5) (Figure 6B), which also exploits van der Waals contacts with V351. More detailed analysis of Lewis X binding mode shows that here the interaction with V351 is directly established with the 2-OH and C-2 of fucose ring. Indeed, while it is also the 3-OH and 4-OH of the fucose that are implicated in Ca^{2+} coordination, as in mannose-based ligands, here the 4-OH is axial and thus induces the fucose ring to tip over toward V351 (see Figure S5A in the Supporting Information). However, whatever the ligand is (Manα1−2Man, Lewis X, or pseudo-1,2-mannobioside), they all use rigorously the same hydrogen donors and acceptors to interact with their 3-OH and 4-OH (compare Figure S5B for LNFIII and Figure 6). It means that they all have an asymmetrical hydrogen-bonding pattern of the mannose type, in contrast to the symmetrical pattern observed in galactose binding C-type lectins.[38] Thus, hydrogen-bonding partners, of the 3-OH and 4-OH, are not making the differences between the compounds here. Difference in binding is mostly due to their capacity to establish secondary interaction with residues in the vicinity of the Ca^{2+} site, like with the valine 351 for pseudo-1,2-mannobioside and Lewis X.

Interestingly, while several DC-SIGN related C-type lectins, such as DC-SIGNR and langerin, are capable of recognizing mainly mannose-based oligosaccharides, DC-SIGN is specific for Lewis-type carbohydrates as well.[39] In the case of DC-SIGNR, this difference has been previously attributed to the substitution of V351 in DC-SIGN by a serine in DC-SIGNR. Guo et al.[39] showed that a simple mutation reversing this serine to a valine can convert DC-SIGNR to a Lewis X binding lectin. This indicates that Val 351 represents a key residue modulating the specificity of the primary DC-SIGN binding site. The stabilization of **1** through V351 suggests that a similar selectivity exists for our compound.

DC-SIGN/Langerin Specificity. As mentioned above, selectivity is a key concern in the selection of lead compounds for the development of DC-SIGN antagonists. The main issue involves selectivity versus langerin, a C-type lectin known to protect the host against HIV infection, which should not be antagonized by DC-SIGN targeting compounds.[25,32,40]

The specificity of **1a** for DC-SIGN and langerin was evaluated using a previously described surface plasmon resonance (SPR) competition assay.[25,41] **1a** was compared to mannose and to the natural Manα1−2Man disaccharide for its ability to inhibit binding of the extracellular domains (ECD) of DC-SIGN or langerin to a mannosylated BSA (BSA-Man) surface (Figure 7A and B). To evaluate the interaction avidity effect for the lectins, we prepared two flow cells with different BSA-Man density (Fc-HD and Fc-LD in Figure 7 corresponding, respectively, to flow cell of high density and low density). It is evident that BSA-Man density had virtually no effect on the inhibition of DC-SIGN binding, and for this lectin an improvement by a factor of 3 in the apparent affinity was obtained for both Manα1−2Man and **1a** as compared to mannose (Figure 7b, IC_{50} of 885 and 1020 μM, respectively, as compared to 3.05 mM for mannose). Thus, the natural disaccharide and the mimic display the same affinity for DC-SIGN in this assay.

On the contrary, although the general pattern of the compound potencies remained the same for both surfaces (Figure 7B), it was harder to achieve inhibition of langerin binding to the Fc-HD surface (5000 RU) than to the Fc-LD (1350 RU), with a lower BSA-Man density. For instance, at lower Man-BSA density, Manα1−2Man and **1a** have an IC_{50} of 713 and 2760 μM, respectively, that become 1630 and 6827 μM at higher density. This phenomenon depends on the fact that, as previously described and detailed in the experimental section,[25] langerin displays a measurable affinity to the dextran matrix on the chip surface, and thus dextran/BSA-Man surface must be considered as a combined heterogeneous ligand of langerin. The different ratios of dextran and BSA-Man, depending directly from the BSA-Man density, contribute to a complex relative affinity of the surface for langerin.

The dependence of the IC_{50} values on the BSA-Man surface-density in the langerin assay prevented a straightforward comparison of the IC_{50} values obtained for the two lectins. However, comparison of the data in Figure 7b clearly shows that, moving from Manα1−2Man to **1a**, a loss of affinity is observed for langerin while the affinity is conserved for DC-SIGN. An attempt at quantifying the selectivity effect in relative terms is proposed in the Supporting Information (Figure S6). This finding further supports the hypothesis of a relation between DC-SIGN selectivity and the use of a special binding region, shared by Lewis-type derivatives.

The crystal structure of a langerin CRD/Manα1−2Man complex has recently been published.[33] As for DC-SIGN, two binding modes have been observed with alternatively the reducing or the nonreducing mannose involved in the primary binding through Ca^{2+} chelation (see Supporting Information, Figure S7). However, some potential hindrance in the binding

dx.doi.org/10.1021/ja3053305 | J. Am. Chem. Soc. 2013, 135, 2518−2529

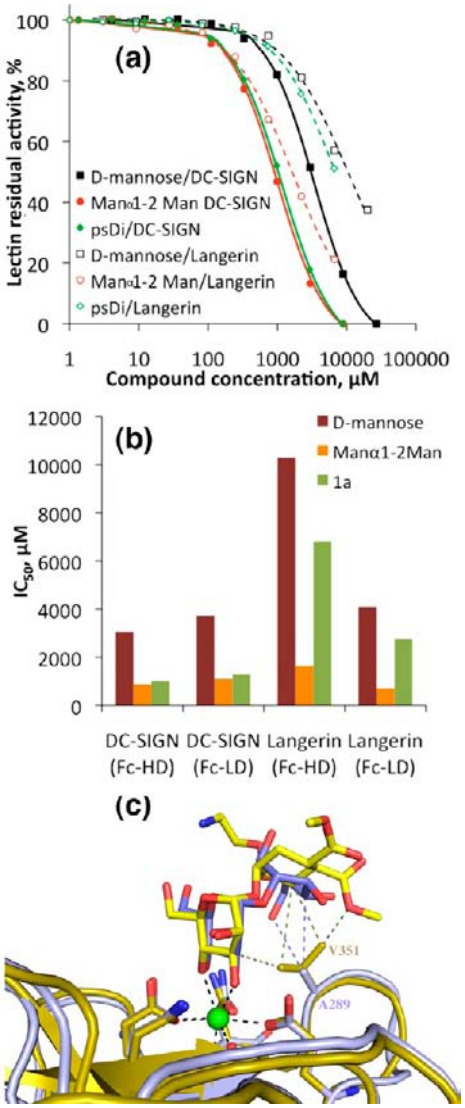

Figure 7. Specificity of pseudo1,2-mannobioside as a function of the C-type lectin. (a) SPR experiment results of the inhibition of DC-SIGN ECD and langerin ECD binding to BSA-Man/dextran surface by mannose, Manα1−2Man, and pseudo-1,2-mannobioside. Results for higher BSA-Man density are represented. (b) Lectins selectivity: IC_{50} histograms for two different flow cells (Fc-HD − 5000 RU, Fc-LD − 1350 RU of immobilized BSA-Man). (c) Superposition of Manα1−2Man/langerin and **1a**/DC-SIGN complex structures. Langerin and D-SIGN backbones are in blue and yellow, respectively. Manα1−2Man and **1a** are represented in blue and yellow. van der Waals interactions of Manα1−2Man, with A289 of langerin, are represented as dashed blue lines, while those of **1a**, with V351 of DC-SIGN, are as dashed yellow lines.

site of langerin, due to Lys 299, implies Manα1−2Man binding modes in the opposite orientations from that observed in DC-SIGN.[33] Thus, the major binding mode of Manα1−2Man to langerin is close to the binding mode of **1** to DC-SIGN (Figure 7c), and the main difference is the Val 351 of DC-SIGN, which is replaced by Ala 289 in langerin (see Figure S7 and Figure 7c). Comparing the major binding mode for the Manα1−2Man/langerin complex and the **1**/DC-SIGN structure, replacement of Ala 289 (in langerin) with Val 351 (in DC-SIGN) significantly increases van der Waals contacts within the complex. Moreover, in langerin, Manα1−2Man establishes a contact with Ala 289 through the hydroxyl group of the C-6 that fills the distance to the methyl of the alanine side chain. This requires previous desolvation of the 6-OH group, an energetically costly process. In the equivalent position, **1** does not have any substituent. Formation of a **1**/langerin complex is disfavored simultaneously due to the loss of a bulky side chain in this position, valine to alanine, and to the absence of a group extending from the cyclohexane ring and capable of establishing van der Waals contact with the alanine side chain. Therefore, as observed previously for the Lewis X DC-SIGN versus DC-SIGNR specificity, Val 351 is making the difference in the specificity of **1** for DC-SIGN, relative to langerin. The replacement by a serine in DC-SIGNR or an alanine in langerin, although being a moderate modification, is sufficient to lose Lewis X specificity in one case and to ensure here a preference of **1** for DC-SIGN with respect to langerin.

CONCLUSIONS

Multiple carbohydrate binding modes have been reported as a mechanism allowing improved affinity toward DC-SIGN.[28] Indeed, it is interesting to note that in our assay **1** presents the same IC_{50} as Manα1−2Man, while it has only a unique binding mode. This suggests that intrinsically **1** binds stronger than each individual binding mode of Manα1−2Man. Trying to mimic Manα1−2Man, which is also a good ligand of DC-SIGN, by using a pseudo-1,2-mannobioside, we finally discovered that this molecule mimics Lewis X binding mode to DC-SIGN, by exploiting lipophilic interactions with V351 side chain. Although this was not anticipated, it is a very interesting and convenient result considering that among a wide range of C-type lectins, DC-SIGN is the only one able to bind Lewis X.[42] This result underlines that V351 is a key residue to target for the design of DC-SIGN specific inhibitors. Indeed, this structure suggests that addition of lipophilic groups to the cyclohexane scaffold of **1** should allow one to extend contacts with the protein surface, which might improve the affinity and the DC-SIGN specificity to higher level. Each affinity improvement at the monovalent level will be even more amplified upon grafting onto multivalent presenting scaffolds. Future work in our network is going along this line: the development of DC-SIGN-adapted glycomimics based on a structurally driven approach.

EXPERIMENTAL PROCEDURES

Synthesis of Compounds. *Compound* ***1a***. The synthesis of **1a** was previously described by Sattin et al.[16]

Compound ***1b***. Pseudo-1,2-mannobioside **1c** (10 mg, 0.02 mmol), propargyl alcohol (1.8 mg, 0.03 mmol), CuBr (2.2 mg, 0.015 mmol), and TBTA (1.6 mg, 0.03 mmol) were dissolved in 1 mL of THF/H_2O (1:1). After 18 h, the solvent was evaporated, and the resulting crude was purified by silica gel column chromatography (CH_2Cl_2/MeOH 9.5:0.5, 8.5:1.5, 8:2), affording 8.3 mg (75% yield) of compound **1b** as an oil. ^{1}H NMR (D_2O) 300 MHz δ ppm: 8.06 (s, 1H, $H_{triazol}$), 4.96 (d, 1H, J_{1-2} = 1.64 Hz, H-1_{mann}), 4.79 (s, 2H, CH_2OH), 4.64 (t, J = 4.8 Hz, 2H, CH_2N), 4.01−3.93 (m, 3H, OCH_2CH_2N, H-2_{mann}), 3.90−3.84 (m, 2H, CHOCH_{mann}, H-6_{mann}), 3.83−3.78 (m, 1H, H-3_{mann}), 3.76−3.66 (m, 8H, CHOCH_2CH_2N, H-$6'_{mann}$, CH_3), 3.63−3.57 (m, 2H, H-4_{mann}, H-5_{mann}), 2.90−2.79 (m, 1, CHCOOCH_3), 2.47−2.35 (m, 1, CHCOOCH_3), 2.06−1.96 (m, 2H, CH_{2eq}C, CH_{2eq}C), 1.79−1.68 (m, 1H, CH_{2ax}C), 1.51−1.39 (m, 1H, CH_{2ax}C). ^{13}C NMR (D_2O) 75 MHz δ ppm: 177.4, 177.2 (C=O), 146.8 ($C_{triazol}$), 124.6 (C$H_{triazol}$), 98.5 (C-1_{mann}), 73.7 (C-5_{mann}), 73.4 (CHOCH_2CH_2N), 70.8 (C-3_{mann}), 70.3 (OCH_2CH_2N, C-2_{mann}), 66.7 (C-4_{mann}), 66.5 (CHOCH), 60.9 (C-6_{mann}), 54.6 (CH_2OH), 52.5 (CH_3O), 50.3 (OCH_2CH_2N), 38.8 (CHCOOCH_3), 38.6 (CHCOOCH_3), 26.5 (CCH_2C), 26.4 (CCH_2C). $[\alpha]^{25}_D$ = +27.1° (c 0.6, MeOH). ESI−

dx.doi.org/10.1021/ja3053305 | J. Am. Chem. Soc. 2013, 135, 2518−2529

MS calcd for $C_{21}H_{33}N_3O_{12}Na$ (m/z), 542.2; found, 541.9 $[M + Na]^+$. HRMS (FAB) calcd for $C_{21}H_{33}N_3O_{12}Na$ (m/z), 542.1962; found, 542.1979 $[M + Na]^+$.

Cloning and Expression of Recombinant DC-SIGN S-CRD. The sequence coding for carbohydrate recognition domain of DC-SIGN, comprising amino acids 254−404, was obtained by PCR using the forward primer 5′-gcattaggtctctgcgcatgcacccctgtccctggga-3′ and the reverse primer 5′-gcagcaggtctcttatcactacgcaggagggggtttg-3′. The PCR template used was a previous construct for DC-SIGN ECD overexpression, which has been described previously.[8] The PCR product was inserted into pASK-IBA7plus vector (IBA GmbH), at the Bsa I sites, in phase with a Strep-Tag II sequence and a factor Xa cleavage site, both located at the N-terminal end of the protein (the CRD with this N-terminal tag will be called hereafter S-CRD). The resulting plasmid was sequence checked and used to transform calcium competent *E. coli* BL21(DE3).

Culture was initiated from a 5% dilution of an overnight culture into LB medium with 100 mg/L ampicillin. Cells were grown for 3 h at 37 °C, and DC-SIGN S-CRD expression was induced by addition of 1 mg/L anhydrotetracycline for 4 additional hours. Cells were harvested by centrifugation at 5000*g* for 20 min. The protein was expressed as inclusion bodies, and then a refolding step was required prior to the purification procedures.

Protein Purification. The pellet, containing DC-SIGN S-CRD, obtained from a 1 L culture was resuspended in 30 mL of buffer A (150 mM NaCl and 25 mM Tris pH 8). Cells were lysed by freezing at −20 °C, thawing, and sonication with addition of a tablet of protease inhibitors (Roche Diagnostics). Inclusion bodies were isolated by centrifugation at 100 000*g* for 30 min at 4 °C, and using a Potter-Elvehjem homogenizer were resuspended in 30 mL of buffer A supplemented with 2 M urea and 1% Triton X-100, and recovered by a second centrifugation. Inclusion bodies were washed again with buffer A and solubilized in buffer A supplemented with 6 M guanidine hydrochloride and 0.01% 2-mercaptoethanol. Inclusion bodies solution was centrifuged at 100 000*g* for 1 h at 4 °C, supernatant was diluted in 120 mL of buffer of 1.25 M NaCl, 25 mM Tris pH 8, and 25 mM $CaCl_2$, and the resulting solution was dialyzed overnight against 880 mL of buffer of 25 mM Tris pH 8. Refolding of inclusion bodies was achieved by extensive dialysis in buffer A supplemented with 4 mM $CaCl_2$ (buffer A′), and insoluble compounds were removed by the last centrifugation step at 100 000*g* for 1 h at 4 °C.

Purification was then performed as previously described for langerin S-CRD.[43] Briefly, the first step of DC-SIGN S-CRD purification was performed by affinity chromatography on a 15 mL Strep-Tactin superflow column (IBA GmbH) equilibrated in buffer A′ and eluted in the same buffer supplemented with 2.5 mM desthiobiotin. A second purification step was performed with DC-SIGN S-CRD-containing fractions concentrated to 1.5 mL. Functional DC-SIGN S-CRD was separated from nonfunctional protein as it was delayed on a 15 mL mannose-agarose column equilibrated in buffer A′. Functional DC-SIGN S-CRD-containing fractions were concentrated to 11 mg/mL.

DC-SIGN ECD and Langerin ECD were produced and purified as previously described.[8,44]

DC-SIGN CRD Crystallization. Crystallization assays were performed manually by hanging-drop vapor-diffusion method at 293 K in EasyXtal plates (Qiagen) with protein−carbohydrate stock solution made by mixing 10 μL of concentrated DC-SIGN S-CRD with 1 μL of 100 mM pseudo-1,2-mannobioside **1a**. Drops, prepared by mixing 1 μL of reservoir solution with 1 μL of protein−carbohydrate stock solution, were equilibrated against 1 mL of reservoir solution. The best crystals appeared when reservoir solution was composed of 20% PEG 3350, 100 mM cacodylate pH 6.5, and 200 mM NaCl. A 0.06 × 0.06 × 0.65 mm crystal was cryoprotected in Paratone-N (Hampton Research) and was flash-frozen in liquid nitrogen.

Data Collection and Processing. X-ray diffraction data were collected at ID29 beamline at ESRF Grenoble. Two data sets were collected at a wavelength of 0.9809 Å, with a crystal-to-detector distance set to 197.89 mm and an X-ray transmission of 8.1%. The first data set was collected at maximal resolution and the second with reduced exposure time to minimize detector saturation at lower resolution. The first data set, composed of 360 images, was collected with an oscillation range of 0.5° per image and an exposure time of 1 s. The second data set, composed of 120 images, was collected with an oscillation range of 3° per image and an exposure time of 0.2 s.

Data sets were processed and merged using the programs XDS and XSCALE, respectively.[45] Statistics of data processing are summarized in Table 1. Matthews coefficient was calculated using the program MATTHEWS_COEF.[46]

Table 1. DC-SIGN CRD/Pseudo-1,2-mannobioside 1a Complex Data Collection and Structure Refinement Statistics

Data Collection Statistics	
wavelength (Å)	0.9809
space group	$P4_32_12$
unit cell parameters (Å)	$a = b = 71.45$; $c = 52.67$
resolution (Å)	42.41−1.42 (1.46−1.42)[a]
measured reflns	658 501 (12 715)
unique reflns	25 925 (1761)
completeness (%)	99.4 (92.4)
I/σ (I)	28.67 (5.56)
R_{merge}[b] (%)	13.0 (58.0)
Structure Refinement Statistics	
resolution (Å)	42.41−1.42 (1.46−1.42)
refinement factors	
used reflns/free (%)	24628/5.0
R_{cryst}[c]	0.145
R_{free}[c]	0.172
rmsd from ideality	
bond lengths (Å)	0.030
bond angles (deg)	2.413
Ramachandran plot (%)	
most favored regions	87.0
additional allowed regions	11.3
generously allowed regions	1.7
disallowed regions	0.0
average B-factor (Å^2)	13.30

[a]Values in parentheses are for the highest resolution shell. [b]$R_{merge} = \sum_h\sum_m|I_m(h) - \langle I(h)\rangle|\sum_h\sum_m I_m(h)$. [c]$R_{cryst} = \sum||F_0| - |F_c||\sum|F_0|$, and $R_{free} = R_{cryst}$ calculated with 5% of F_0 sequestered before refinement.

Phasing, Model Building, and Structure Refinement. Phasing was performed by molecular replacement with a model built from a structure of DC-SIGN CRD (pdb code: 2IT6) depleted of calcium ions, carbohydrate molecules, and water molecules. The best solution resulting from molecular replacement was used as the starting model for structure refinement. The structure refinement was performed by cycling between manual building using the program COOT[46] and energy minimization with the program REFMAC 5 from the CCP4 package.[46] Geometry of the structure was verified using Procheck program with check module of the CCP4 program suite. Finally, the structure was verified twice using validation tools of the PDB, before submission, using the PDB ADIT deposition tool (http://deposit.rcsb.org/adit/) and during deposition procedure by PDB staff members. Statistics of structure refinement are summarized in Table 1. The crystal structure of DC-SIGN CRD/**1a** has been deposited in Protein Data Bank under PDB code 2xr5.

Surface Plasmon Resonance Experiments. Surface plasmon resonance experiments were performed on a Biacore 3000 using a CM4 chip, functionalized at 5 μL/min. Flow cells (Fc) 1, 2, and 3 were activated with 50 μL of an 0.2 M EDC/0.05 M NHS mixture; after this step, Fc2 and Fc3 were functionalized with mannosylated bovine serum albumine (BSA-Man), and finally the remaining activated groups of both flow cells were blocked with 30 μL of 1 M

dx.doi.org/10.1021/ja3053305 | J. Am. Chem. Soc. 2013, 135, 2518−2529

Table 2. Comparison of Interproton Distances of 1b in Bound State Obtained from NMR Data in Solution and from Measurement on the Crystal Structure

proton pair	distances from TR-NOESY (Å)[a]	distances from X-ray (Å)[b]
	Intraresidual	
$H3_{ax}/H3_{eq}(C)$	1.7	1.8
H5/H1(C)	3.5	3.7
$H6_{eq}/H1(C)$	2.5	2.5
$H6_{ax}/H1(C)$	2.4	2.4
	Inter-residual	
$H1(M)/H3_{eq}(C)$	2.6[c]	2.3
H1(M)/H2(C)	2.3	2.5
H1(M)/H4(C)	3.3	3.5
$H2(M)/H6_{ax}(C)$	4.2	4.3
$H2(M)/H3_{eq}(C)$	3.2	3.9
H2(M)/H4(C)	3.1	3.3
$H3(M)/H6_{ax}(C)$	3.4	3.4
H3(M)/H4(C)	4.4	4.0

[a]Distances derived using the isolated spin-pair approximation (ISPA) by comparing relative NOE intensities with that of the reference (H3ax−H3eq of cyclohexyl ring of **1b**). [b]Distances measured on ligand protons added onto the X-ray structure with Pymol 1.2. [c]Overlapping of H3eq(C) diagonal peak is affecting this measurement. As a result, this distance is slightly overestimated.

ethanolamine. After blocking, the three flow cells were treated with 10 μL of 10 mM HCl to remove unspecific bound proteins and 20 μL of 50 mM EDTA to expose surface to regeneration protocol. After these steps, 5000 RU and 1170 RU of BSA-Man were immobilized on the surfaces of Fc2 and Fc3, respectively. BSA-Man stock solution was prepared by dissolving the glycoprotein in water to a final 1 mg/mL concentration, and for immobilization it was diluted to 60 μg/mL in a buffer of 10 mM sodium acetate pH 4.

To control surface activity and to determine optimal working protein concentration, 13 μL of samples of increasing concentrations of DC-SIGN and langerin ECDs (0.7−46.7 μM for DC-SIGN, and 0.7−45.7 μM for langerin) was injected onto the surfaces. The selected concentration was 20 μM for both lectins.

For inhibition studies, samples of each lectin mixed with increasing concentrations of inhibiting compounds were prepared in a running buffer (buffer A′ supplemented with 0.005% P20 surfactant), and 13 μL of each sample was injected onto the surfaces at a 5 μL/min flow rate. Concentrations of inhibiting compounds ranged from 4.1 to 26 667 μM or from 3.1 to 20 000 μM for D-mannose, from 4.1 to 8889 μM or from 1.0 to 6667 μM for Manα1−2Man, and from 1.3 to 8782 μM or from 1.0 to 6587 μM for pseudo-1,2-mannobioside **1a** mixed with DC-SIGN or langerin ECDs, respectively. The resulting sensorgrams were reference surface corrected, except in the case of langerin, because this lectin displayed affinity to the dextran matrix, and thus dextran/BSA-Man surface was considered as a combined ligand of langerin (as described previously in Andreini et al).[25]

$$y = R_{hi} - \frac{R_{hi} - R_{lo}}{1 + \left(\frac{conc}{A_1}\right)^{A_2}} \quad (1)$$

$$IC_{50} = A_1 \cdot \left(\frac{R_{hi} - R_{lo}}{R_{hi} - 50} - 1\right)^{1/A_2} \quad (2)$$

The lectin binding responses were extracted from the sensorgrams, converted to percent residual activity values (y) with respect to lectin alone binding, and plotted against corresponding compound concentration. The four-parameter logistic model (eq 1) was fitted to the plots, and the IC_{50} values were calculated using the values of fitted parameters (R_{hi}, R_{lo}, A_1, and A_2) and eq 2.

NMR Spectroscopy Experiments. NMR spectroscopy experiments were performed on a Bruker Avance DRX 500 MHz spectrometer equipped with a 5 mm inverse triple-resonance probe head. NMR samples were prepared in 550 μL of 99.9% D_2O and for the experiments in the presence of the receptor, in buffer D_2O (150 mM NaCl, 4 mM $CaCl_2$, 25 mM d-Tris, pD 8), and with 19 μM DC-SIGN ECD. The concentration of the ligand was 1.35 mM, and the same sample was used for both STD NMR and TR-NOESY experiments. For the two-ligand equimolar competition experiment, a concentration of 1.7 mM was employed.

STD NMR experiments were carried out at 10, 25, and 35 °C, by using a train of Gaussian shaped pulses of 49 ms (field strength of ca. 80 Hz), an interpulse delay of 1 ms,[47] and 15 ms spin-lock pulse (field strength of 3.7 kHz) prior to acquisition. The on-resonance frequency was set to 0 ppm, and the off-resonance frequency was 40 ppm. Appropriate blank experiments were used to ensure the lack of direct saturation of the ligand protons. Saturation times of 0.5, 1, 1.5, 2, 3, 4, and 5 s were used to obtain the STD build-up curves.

The binding epitope was characterized by the analysis of initial slopes of the STD intensities at 25 °C:[48] the experimental $(I_0 - I_{sat}/I_0)$ curves were fitted to an exponential function described by the equation $STD(t_{sat}) = STD_{max}(1 - e^{-ksat \cdot tsat})$, which allows one to calculate STD at zero saturation time (initial slopes) by multiplying the resulting parameters STD_{max} and k_{sat}.[49] The epitope is obtained by normalization of the whole set of initial slopes against the highest value, and expressing the result in percentage.

NOESY experiments were carried out using a phase-sensitive pulse program with gradient pulses in the mixing time and with presaturation.[50,51] Mixing times of 0.2, 0.3, 0.4, 0.5, 0.6, and 0.8 s were used for NOESY spectra and 0.1, 0.2, 0.3, and 0.5 s for TR-NOESY spectra. NOE build-up curves were obtained from the normalized cross-peak volumes (ratio cross peak over diagonal peak) as a function of the mixing time. For TR-NOESY experiments, the growth was approximately linear up to 300 ms (see Figure S8 in the Supporting Information). Longitudinal cross-relaxation rates were obtained by averaging the ratio of the normalized volume and the mixing time, for mixing times 0.1, 0.2, and 0.3 s. From them, intramolecular ligand proton−proton distances were obtained by using the ISPA approach (isolated spin pair approximation), and taking the distance H3eq−H3ax of the cyclohexyl ring as a reference.

CORCEMA-ST. The Cartesian coordinates of the crystal structure of the complex DC-SIGN CRD/**1a** were employed for the full relaxation matrix calculations. As no chemical shift assignment of the protein protons was available, they were predicted by using the program SHIFTX.[52] Although the experimental irradiation frequency for selective saturation was established at 0 ppm, all of the protein protons with chemical shifts predicted to be within the [0.7, −0.7] ppm range were included, as SHIFTX does not consider the effects of line broadening under the experimental conditions. All exchangeable hydrogen atoms were excluded in the calculations, as the STD NMR experiments were performed in D_2O. We assumed that pdb coordinates for the bound and free protein were identical, and several cycles were performed to reach the optimized parameters. For this protein−ligand system, the classical assumption of an association step limited by diffusion (on-rate 10^8 M^{-1} s^{-1}) was considered. The off-rate was varied within a range (1−100 kHz) that yielded a final dissociation constant within the micromolar range, typical for this kind of ligands of DC-SIGN. No large variations were observed for the R-factor during this process, and the final off-rate was 40 kHz. Assuming a spherical shape for the protein tetramer, the correlation time of bound ligand was set to 115 ns, whereas 0.5 ns was used for the free ligand, and 10 ps for the internal correlation time of methyl groups. This might be considered an oversized value for the correlation time of a protein of about 155 kDa (DC-SIGN tetramer). Nevertheless, this seems to be not uncommon in CORCEMA-ST calculations,[53−55] particularly when the protein shape deviates from a perfect globular shape, as is the case with the DC-SIGN tetramer. To reduce the dimensions of the matrixes, a cut off of 8 Å from the ligand was used. The STD intensities for each binding mode were calculated as percentage fractional intensity changes, $S_{calc,k}$, from the intensity matrix

dx.doi.org/10.1021/ja3053305 | J. Am. Chem. Soc. 2013, 135, 2518−2529

$I(t)$ ($S_{calc,k}$ = (([(I_{0k} − $I(t)_k$)*100]/I_{0k}), where k is a particular proton in the complex, and I_{0k} its thermal equilibrium value),[34] and the calculation was carried out for the set of saturation times experimentally measured (0.5, 1, 1.5, 2, 3, 4, and 5 s). The theoretical STD values were compared to the experimental ones using the NOE R-factor[35,36] defined as:

$$\sqrt{\frac{\sum Wk(\mathrm{STD}_k^{\mathrm{exp}} - \mathrm{STD}_k^{\mathrm{calc}})^2}{\sum Wk(\mathrm{STD}_k^{\mathrm{exp}})^2}}$$

In this equation, $\mathrm{STD}_k^{\mathrm{exp}}$ and STD_k^{calc} refer to experimental and calculated STD values for proton k. The best agreement with experimental data was achieved using conformation B of the residue V351.

■ ASSOCIATED CONTENT

Supporting Information

Complementary analysis of X-ray structures, NMR data (STD spectra, 1D NOESY, etc.), and a formalism to quantify, from the SPR data, the selectivity improvement obtained from one compound to another. This material is available free of charge via the Internet at http://pubs.acs.org.

■ AUTHOR INFORMATION

Corresponding Author

fieschi@ibs.fr

Author Contributions

[∇]These authors contributed equally.

Notes

The authors declare no competing financial interest.

■ ACKNOWLEDGMENTS

We are grateful to Sidaction: Ensemble contre le SIDA for M.T.'s postdoctoral grant and support, and EU ITN Marie-Curie program (CARMUSYS − Grant no. 213592) for funding Cinzia Guzzi, Ieva Sutkeviciute, Renato Ribeiro-Viana, and Norbert Varga. J.A. acknowledges financial support from the MICINN through the Ramon y Cajal program.

■ REFERENCES

(1) Banchereau, J.; Steinman, R. M. *Nature* **1998**, *392*, 245−252.
(2) Bell, D.; Young, J. W.; Banchereau, J. *Adv. Immunol.* **1999**, *72*, 255−324.
(3) van Kooyk, Y.; Engering, A.; Lekkerkerker, A. N.; Ludwig, I. S.; Geijtenbeek, T. B. *Curr. Opin. Immunol.* **2004**, *16*, 488−493.
(4) Geijtenbeek, T. B.; Kwon, D. S.; Torensma, R.; van Vliet, S. J.; van Duijnhoven, G. C.; Middel, J.; Cornelissen, I. L.; Nottet, H. S.; KewalRamani, V. N.; Littman, D. R.; Figdor, C. G.; van Kooyk, Y. *Cell* **2000**, *100*, 587−597.
(5) van Kooyk, Y.; Geijtenbeek, T. B. *Nat. Rev. Immunol.* **2003**, *3*, 697−709.
(6) Geijtenbeek, T. B.; van Kooyk, Y. *Apmis* **2003**, *111*, 698−714.
(7) Hodges, A.; Sharrocks, K.; Edelmann, M.; Baban, D.; Moris, A.; Schwartz, O.; Drakesmith, H.; Davies, K.; Kessler, B.; McMichael, A.; Simmons, A. *Nat. Immunol.* **2007**, *8*, 569−577.
(8) Tabarani, G.; Thépaut, M.; Stroebel, D.; Ebel, C.; Vivès, C.; Vachette, P.; Durand, D.; Fieschi, F. *J. Biol. Chem.* **2009**, *284*, 21229−21240.
(9) Tabarani, G.; Reina, J. J.; Ebel, C.; Vivès, C.; Lortat-Jacob, H.; Rojo, J.; Fieschi, F. *FEBS Lett.* **2006**, *580*, 2402−2408.
(10) Martínez-Avila, O.; Hijazi, K.; Marradi, M.; Clavel, C.; Campion, C.; Kelly, C.; Penadés, S. *Chemistry* **2009**, *15*, 9874−9888.
(11) Becer, C. R.; Gibson, M. I.; Geng, J.; Ilyas, R.; Wallis, R.; Mitchell, D. A.; Haddleton, D. M. *J. Am. Chem. Soc.* **2010**, *132*, 15130−15132.
(12) Ciobanu, M.; Huang, K.-T.; Daguer, J.-P.; Barluenga, S.; Chaloin, O.; Schaeffer, E.; Mueller, C. G.; Mitchell, D. A.; Winssinger, N. *Chem. Commun.* **2011**, *47*, 9321−9323.
(13) Cambi, A.; de Lange, F.; van Maarseveen, N. M.; Nijhuis, M.; Joosten, B.; van Dijk, E. M.; de Bakker, B. I.; Fransen, J. A.; Bovee-Geurts, P. H.; van Leeuwen, F. N.; Van Hulst, N. F.; Figdor, C. G. *J. Cell Biol.* **2004**, *164*, 145−155.
(14) de Bakker, B. I.; de Lange, F.; Cambi, A.; Korterik, J. P.; van Dijk, E. M.; Van Hulst, N. F.; Figdor, C. G.; Garcia-Parajo, M. F. *ChemPhysChem* **2007**, *8*, 1473−1480.
(15) Martínez-Avila, O.; Bedoya, L. M.; Marradi, M.; Clavel, C.; Alcamí, J.; Penadés, S. *ChemBioChem* **2009**, *10*, 1806−1809.
(16) Sattin, S.; Daghetti, A.; Thépaut, M.; Berzi, A.; Sánchez-Navarro, M.; Tabarani, G.; Rojo, J.; Fieschi, F.; Bernardi, A. *ACS Chem. Biol.* **2010**, *5*, 301−312.
(17) Wang, S.-K.; Liang, P.-H.; Astronomo, R. D.; Hsu, T.-L.; Hsieh, S.-L.; Burton, D. R.; Wong, C.-H. *Proc. Natl. Acad. Sci. U.S.A.* **2008**, *105*, 3690−3695.
(18) Luczkowiak, J.; Sattin, S.; Sutkeviciute, I.; Reina, J. J.; Sánchez-Navarro, M.; Thépaut, M.; Martinez-Prats, L.; Daghetti, A.; Fieschi, F.; Delgado, R.; Bernardi, A.; Rojo, J. *Bioconjugate Chem.* **2011**, *22*, 1354−1365.
(19) Lasala, F.; Arce, E.; Otero, J. R.; Rojo, J.; Delgado, R. *Antimicrob. Agents Chemother.* **2003**, *47*, 3970−3972.
(20) Borrok, M. J.; Kiessling, L. L. *J. Am. Chem. Soc.* **2007**, *129*, 12780−12785.
(21) Tran, T. H.; Baz, El, R.; Cuconati, A.; Arthos, J.; Jain, P.; Khan, Z. K. *J. Antivirals Antiretrovirals* **2011**, *3*, 49−54.
(22) Reina, J. J.; Sattin, S.; Invernizzi, D.; Mari, S.; Martinez-Prats, L.; Tabarani, G.; Fieschi, F.; Delgado, R.; Nieto, P. M.; Rojo, J.; Bernardi, A. *ChemMedChem* **2007**, *2*, 1030−1036.
(23) Mitchell, D. A.; Jones, N. A.; Hunter, S. J.; Cook, J.; Jenkinson, S. F.; Wormald, M. R.; Dwek, R. A.; Fleet, G. W. J. *Tetrahedron: Asymmetry* **2007**, *18*, 1502−1510.
(24) Garber, K. C. A.; Wangkanont, K.; Carlson, E. E.; Kiessling, L. L. *Chem. Commun.* **2010**, *46*, 6747−6749.
(25) Andreini, M.; Doknic, D.; Sutkeviciute, I.; Reina, J. J.; Duan, J.; Chabrol, E.; Thépaut, M.; Moroni, E.; Doro, F.; Belvisi, L.; Weiser, J.; Rojo, J.; Fieschi, F.; Bernardi, A. *Org. Biomol. Chem.* **2011**, *9*, 5778−5786.
(26) Berzi, A.; Reina, J. J.; Ottria, R.; Sutkeviciute, I.; Antonazzo, P.; Sánchez-Navarro, M.; Chabrol, E.; Cetin, I.; Rojo, J.; Fieschi, F.; Bernardi, A.; Clerici, M. *AIDS* **2012**, *26*, 127−137.
(27) Mari, S.; Posteri, H.; Marcou, G.; Potenza, D.; Micheli, F.; Jiménez-Barbero, J.; Bernardi, A. *Eur. J. Org. Chem.* **2004**, 5119−5225.
(28) Feinberg, H.; Castelli, R.; Drickamer, K.; Seeberger, P. H.; Weis, W. I. *J. Biol. Chem.* **2007**, *282*, 4202−4209.
(29) Angulo, J.; Díaz, I.; Reina, J. J.; Tabarani, G.; Fieschi, F.; Rojo, J.; Nieto, P. M. *ChemBioChem* **2008**, *9*, 2225−2227.
(30) Guzzi, C.; Angulo, J.; Doro, F.; Reina, J. J.; Thépaut, M.; Fieschi, F.; Bernardi, A.; Rojo, J.; Nieto, P. M. *Org. Biomol. Chem.* **2011**, *9*, 7705−7712.
(31) Valladeau, J.; Ravel, O.; Dezutter-Dambuyant, C.; Moore, K.; Kleijmeer, M.; Liu, Y.; Duvert-Frances, V.; Vincent, C.; Schmitt, D.; Davoust, J.; Caux, C.; Lebecque, S.; Saeland, S. *Immunity* **2000**, *12*, 71−81.
(32) de Witte, L.; Nabatov, A.; Geijtenbeek, T. B. H. *Trends Mol. Med.* **2008**, *14*, 12−19.
(33) Feinberg, H.; Taylor, M. E.; Razi, N.; Mcbride, R.; Knirel, Y. A.; Graham, S. A.; Drickamer, K.; Weis, W. I. *J. Mol. Biol.* **2011**, *405*, 1027−1039.
(34) Jayalakshmi, V.; Rama Krishna, N. *J. Magn. Reson.* **2004**, *168*, 36−45.
(35) Xu, Y.; Sugár, I. P.; Krishna, N. R. *J. Biomol. NMR* **1995**, *5*, 37−48.
(36) Krishna, N. R.; Agresti, D. G.; Glickson, J. D.; Walter, R. *Biophys. J.* **1978**, *24*, 791−814.
(37) The spin diffusion process led to an apparent increase of weak intra-residual NOEs (H3ax(C)−H4(C), H6ax(C)−H5(C), H2(M)−

H4(M), or H2(M)−H5(M)), and an apparent decrease of strong intra-residual NOEs (H3ax(C)−H5(C) or H6ax(C)−H4(C)), which can be observed as differences in some cross peaks between both spectra in Figure 5. For a complete explanation of these effects, see: Ni, F. *Prog. Nucl. Magn. Reson. Spectrosc.* **1994**, *26*, 517−606. In view of that, only strong inter-residual NOEs were considered in the analysis.

(38) Zelensky, A. N.; Gready, J. E. *FEBS J.* **2005**, *272*, 6179−6217.

(39) Guo, Y.; Feinberg, H.; Conroy, E.; Mitchell, D. A.; Alvarez, R.; Blixt, O.; Taylor, M. E.; Weis, W. I.; Drickamer, K. *Nat. Struct. Mol. Biol.* **2004**, *11*, 591−598.

(40) de Witte, L.; Nabatov, A.; Pion, M.; Fluitsma, D.; de Jong, M. A. W. P.; de Gruijl, T.; Piguet, V.; van Kooyk, Y.; Geijtenbeek, T. B. H. *Nat. Med.* **2007**, *13*, 367−371.

(41) Timpano, G.; Tabarani, G.; Anderluh, M.; Invernizzi, D.; Vasile, F.; Potenza, D.; Nieto, P. M.; Rojo, J.; Fieschi, F.; Bernardi, A. *ChemBioChem* **2008**, *9*, 1921−1930.

(42) Lee, R. T.; Hsu, T.-L.; Huang, S. K.; Hsieh, S.-L.; Wong, C.-H.; Lee, Y. C. *Glycobiology* **2011**, *21*, 512−520.

(43) Thépaut, M.; Vivès, C.; Pompidor, G.; Kahn, R.; Fieschi, F. *Acta Crystallogr., Sect. F* **2008**, *64*, 115−118.

(44) Thépaut, M.; Valladeau, J.; Nurisso, A.; Kahn, R.; Arnou, B.; Vivès, C.; Saeland, S.; Ebel, C.; Monnier, C.; Dezutter-Dambuyant, C.; Imberty, A.; Fieschi, F. *Biochemistry* **2009**, *48*, 2684−2698.

(45) Kabsch, W. *J. Appl. Crystallogr.* **1993**, *26*, 795−800.

(46) Collaborative Computational Project, No. 4.. *Acta Crystallogr., Sect. D* **1994**, *50*, 760−763.

(47) Mayer, M.; Bernd, M. *Angew. Chem., Int. Ed.* **1999**, *38*, 1784−1788.

(48) Mayer, M.; Meyer, B. *J. Am. Chem. Soc.* **2001**, *123*, 6108−6117.

(49) Mayer, M.; James, T. L. *J. Am. Chem. Soc.* **2004**, *126*, 4453−4460.

(50) Jeener, J.; Meier, B. H.; Bachmann, P.; Ernst, R. R. *J. Chem. Phys.* **1979**, *71*, 4546−4553.

(51) Wagner, R.; Berger, S. *J. Magn. Reson., Ser. A* **1996**, *123*, 119−121.

(52) Neal, S.; Nip, A. M.; Zhang, H.; Wishart, D. S. *J. Biomol. NMR* **2003**, *26*, 215−240.

(53) Yuan, Y.; Bleile, D. W.; Wen, X.; Sanders, D. A. R.; Itoh, K.; Liu, H.-W.; Pinto, B. M. *J. Am. Chem. Soc.* **2008**, *130*, 3157−3168.

(54) Kemper, S.; Patel, M. K.; Errey, J. C.; Davis, B. G.; Jones, J. A.; Claridge, T. D. W. *J. Magn. Reson.* **2010**, *203*, 1−10.

(55) Canales, A.; Rodríguez-Salarichs, J.; Trigili, C.; Nieto, L.; Coderch, C.; Andreu, J. M.; Paterson, I.; Jiménez-Barbero, J.; Díaz, J. F. *ACS Chem. Biol.* **2011**, *6*, 789−799.